Research Article

Silver nanoparticles synthesized from *Aloe barbadensis* leaf extract induces G0/G1 cell cycle arrest in THP-1 acute monocytic leukemia cells

Narayanan Santhanam[1], Aravind Arivazhagan[1], Krithiga Mohan Kennedy[2], Subhashini Swaminathan[1]*

[1]*Department of Biotechnology, SRM Institute of Science and Technology, Chennai, Tamil Nadu, India.*

[2]*College of Pharmacy, SRM Institute of Science and Technology, Chennai, Tamil Nadu, India.*

Received: 21 January 2019 Revised: 22 February 2019 Accepted: 2 March 2019

Abstract

Objective: The purpose of this study is to synthesize silver nanoparticles using *Aloe barbadensis* leaf extract by green chemistry approach and to determine the anti-cancer activity of synthesized silver nanoparticles on THP-1 acute monocytic leukemia cells. **Material and methods:** The *Aloe barbadensis* leaf was analysed for its phytoconstituents using biochemical test which revealed presence of many important phytocompounds. The nanoparticles were then synthesized using leaf extract and characterized by UV-vis spectroscopy, FTIR, XRD, zeta potential, FESEM and EDX which revealed that nanoparticles possess FCC structure with size ranging from 6 nm to 24 nm. **Results and conclusion:** The *in-vitro* antileukemic activity was determined by MTT assay on THP-1 cell lines which showed significant cell death in concentration dependent manner. The DAPI staining and arcidine orange/ethidium bromide dual staining showed apoptotic nuclei in silver nanoparticles treated cells. The Annexin V FITC/PI analysis using flow cytometry showed increase in apoptotic cell population in concentration dependent manner and cell cycle analysis showed cell cycle arrest at Sub G0/G1 phase. DCFDA dye staining revealed increase in intracellular ROS followed by rhodamine 123/PI staining which revealed depolarization of mitochondria. The caspase 3 level was upregulated indicating that the synthesized silver nanoparticles induce caspase 3 mediated apoptosis in THP-1 cells *in-vitro* and caspase 3 activity was confirmed by DNA fragmentation ladder assay which showed fragmentation of DNA.Our results show that green synthesis of silver nanoparticles synthesized using *Aloe barbadensis* leaf extract is eco-friendly, cost efficient, convenient and inhibited the proliferation of THP-1 leukemia cells indicating the potential use of *Aloe barbadensis* mediated silver nanoparticles has potential to develop as nano drug for leukemia therapy.

Keywords: Silver nanoparticles, green synthesis, *Aloe vera*, leukemia, anticancer, apoptosis, flow cytometry, biomedical application, nanomedicine

Introduction

Leukemia is a cancer of blood forming tissues which initially originates in bone marrow that leads to overproduction of abnormal white blood cells in the body that couldn't function normally and fight infections like normal white blood cells (National Cancer Institute). The exact cause of leukemia is unknown but it has been reported that ionizing radiation (Lewis and Edward,1957), prior chemotherapy (Kaldor et al., 1990; Curtis et al., 1990) and exposure to potential carcinogen like benzene (Snyder and Robert, 2012) are risk factors of leukemia. Like other cancers, Leukemia is also triggered by certain mutations (Yan et al., 2011) in DNA like activation of oncogenes and deactivation of tumour suppressor genes which can disrupt the normal cell division thereby avoiding DNA repair mechanism and apoptosis. The current treatments include radiation therapy (Duffner and Patrica, 2004), chemotherapy (Foon et al., 1981), bone marrow transplantation (Horowitz et al., 1990) and targeted therapy (Deininger et al., 2003). Leukemia is mainly classified in to acute leukemia and chronic leukemia which can be further classified in to many sub-types. But whatever type of leukemia it is, the current treatments have many limitations. The radiation therapy has good efficiency only at initial stage

Address for Corresponding Author:
Subhashini Swaminthan
Department of Biotechnology, SRM Institute of Science and Technology, Chennai, Tamil Nadu, India
Email: subhashinikennedy@gmail.com

DOI: https://doi.org/10.31024/ajpp.2019.5.4.8

of leukemia but it affects nearby tissues or organs and also involves arising of many side effects which further increases pain and discomfort for the patients (Al-Mefty et al., 1990). Chemotherapy drugs have poor solubility, bioavailability, non-specific to target cells and mostly results in remission of leukemia which may be resistant to further drug treatment (Holleman et al., 2004). Bone marrow transplantation is an ideal option but its efficiency is not promising due to complex procedure, graft rejection (Horowitz et al., 1990) and very high cost. Hence there is a need of cheap substance or drug that exhibits anti-leukemic activity without much side effects.

Nanotechnology plays an important role in modern research dealing with synthesis of particle's structure with size from 1 to 100 nm range (Khan et al., 2017). These nanoparticles exhibit different properties than other macro particles due to their size property and has more surface area to volume ratio (Beiner et al., 2009). Nanoparticles are gaining huge interest in many large fields such as health care, medical diagnosis and pharmaceutical applications. Out of all nanoparticles created so far, silver nanoparticles are great interest from all researchers due to their properties like anti-bacterial (Jain et al., 2005, Krishnaraj et al., 2010; Rai et al., 2009), anti-septic aiding in wound healing (Tian et al., 2017), anti-viral(Galdiero et al., 2011 and Lara et al., 2010) and anti-fungal activity (Jo et al., 2009; Elumalai et al., 2010). Generally, nanoparticles were created by physical (Lung et al., 2007) and chemical methods (Lu et al., 2002) that pose potential toxicity to normal health. Hence green synthesis of nanoparticles is latest development in today's nanomedicine field. The green synthesis use microbes (Narayanan et al., 2010) or plants (Sharma et al., 2009) to produce assembly of nanoparticles that are cost effective, environment friendly, rapid synthesis in one step process, no complex procedure required, no need of high temperature, energy or pressure and most importantly it exhibits very low toxicity to normal body. However, plant inspired nanoparticle synthesis is preferred over microbial based production as latter requires maintaining microbes at particular condition. Plants release certain phytochemicals that reduces and stabilizes the nanoparticles and hence plant based synthesis of nanoparticles might exhibit synergistic activity of silver and plant compounds. The key factor in selecting a plant for producing nanoparticle is that the plant should possess many medicinal phytocompounds in large quantities so that reduction and stabilization of nanoparticles occur properly and that phytocompounds if present of nanoparticle surface can enhance the anti-leukemic activity. Here, we used *Aloe barbadensis* (aloe vera), a highly regarded medicinal plant (Sahu et al., 2013) that grows prominently in Asia and Africa but now used worldwide as household plant to synthesize silver nanoparticles.

Using metallic nanoparticles has many benefits compared to chemotherapy as nanoparticles are often reported to kill drug resistant cells (Singh et al., 2013) which is a major advantage and also can enter into the cells to disrupt the function of many organelles like nucleus(Rani et al., 2008) and mitochondria resulting in cell death by various pathways. Green synthesis of nanoparticle based anti-leukemic potential is not studied so far and hence we investigated the activity of *Aloe barbadensis* mediated silver nanoparticles towards THP-1 acute monocytic cell lines *in-vitro* and studies its mechanism of action.

Material and methods

Materials and reagents

Silver nitrate (AR grade, CAS- 7761-88-8), Rhodamine123 (CAS- 62669-70-9), Propidium iodide (CAS- 25535-16-4) and Benzene (ACS reagent, CAS- 71-43-2) were purchased from Sigma Aldrich. RPMI (Roswell Park Memorial Institute medium) 1640 (#AL1991), FBS (Fetal Bovine Serum) (#RM10432), Penicillin-Streptomycin antibiotics and Phosphate-buffered saline (PBS) were purchased from HiMedia (Mumbai). MTT [3-(4, 5-Dimethylthiazol-2-Yl)-2, 5-Diphenyltetrazolium Bromide] Reagent (CAS- 298-93-1) was purchased from Merck Millipore. DAPI (4′,6-diamidino-2-phenylindole)(CAS- 28718-90-3), Arcidine Orange (CAS- 65-61-2) and Ethidum Bromide (Cat No:17898) were purchased from Thermo Fisher Scientific. Fluorescein isothiocyanate Annenxin V (Cat No: 51-65874X) and Propidium Iodide (PI) (Cat No. 51-66211E) were purchased from BD Biosciences. DCFDA (2′,7′-Dichlorodihydrofluorescein diacetate, ab113851) and Caspase 3 assay kit (ApoTarget Kit) were purchased from BioSource International, Inc., CA. All other chemicals or reagents used in the study were of analytical grade.

Preparation of leaf extract

Plants were collected from SRM University, Kattankulathur campus and authenticated at Plant Anatomy Research Centre (Reg.No- PARC/2018/3658). 30g portion of leaf was finely cut and made in to powder. The powdered aloe vera leaves were boiled for 15 minutes in 100 ml deionized water followed by cooling at room temperature. Using Whatman No 1 filter paper (Sigma Aldrich), the resultant cooled leaf broth was filtered and stored in a refrigerator at 4°C for further use.

Phytochemical analysis of leaf extract

To evaluate the phytochemical constituents present in the leaf extract, qualitative biochemical tests were carried out. The extract was tested for the presence of carbohydrates (benedicts test), Flavonoids, phenol ($FeCl_2$), tannins ($FeCl_2$), saponins (foam test), glycosides (NaOH test), Alkaloid (HCL test), Resin (acetone test), Steroids

(Salkowski test) and Protiens (biuret test) according to the protocol given in the respective reference articles (Subhashini et al., 2017; Bhandry et al., 2012).

Green synthesis of silver nanoparticles using leaf extract

An aqueous solution (0.01 mM) of silver nitrate ($AgNO_3$) and 5 mg/ml of leaf extract diluted using distilled water was mixed together. After 24 hours, the colour of the resultant solution changed to dark brown from pale yellow which indicates the formation of silver nanoparticles. The resultant brownish solution was centrifuged at 20000 rpm for 15 minutes (3 cycles) and the mixture was collected after discarding the supernatant. The collected silver NP's were allowed to air dry in watch glass and that powder was used for further characterization.

Characterization of synthesized silver nanoparticles

UV–vis spectroscopy (Shimadzu UV/vis 1800 spectrophotometer) was used to study the optical property of synthesized nanoparticles. The nanoparticles were analysed between 200 and 800 nm ranges operated at a resolution of 1nm at room temperature (Haiss et al., 2007). The appearance of peak at 400nm-430nm region confirms the formation of nanoparticles. AgNPs were investigated by Fourier transform IR spectroscopy (FTIR) (PerkinElmer Spectrum RX I Fourier transform IR system) with a frequency ranging from 400 cm-1 to 4000 cm−1 and a resolution of 4 cm−1 using KBr pellet method (Ghule et al., 2006). In order to determine the stability of nanoparticles, 2000 µL of nanoparticle suspension was analysed using Malvern instruments to determine zeta potential (Jiang et al., 2009). XRD (X-ray diffraction) was used to analyse the structure and composition of synthesized silver nanoparticles (Lin et al., 2009). The formation of Ag nanoparticles was determined by an X'Pert Pro X-ray diffractometer (PAN analytical BV) operated with Cu Kα radiation in θ–2θ configurations at a voltage of 40 kV and a current of 30 mA. The images obtained were compared with the Joint Committee on Powder Diffraction Standards (JCPDS) library to determine the crystalline structure. For electron microscopic studies, the images of nanoparticles were studied using FESEM (JSM-6700, JEOL, Japan) (Azizi et al., 2014) by coating 25 µL of sample on copper stub. The fixed samples were coated with carbon and analysed by Energy Dispersive X-Ray (RONTEC's EDX system, Model QuanTax 200, Germany). The FESEM images were than analysed in Image J software to find the mean size of individual nanoparticles.

Cell culture and media preparation

THP-1 acute monocytic leukemia cell line of National Centre for Cell Science (NCCS) origin was a gift from Dr. M. R. Ganesh, IIISM, SRMIST. The cell line was immediately observed for contamination and confluency under phase contrast microscope which revealed no contamination and 70%-75% confluency. The cell lines were then cultured using RPMI 1640 with 10% FBS and 1% antibiotics. Cells were maintained in the media and were allowed to grow in the CO_2 incubator at 35°C with humidified 5% CO_2, 95% air. They were incubated until the flasks attained about 65%-70% confluency. Cells were split 1:4 every 3 days.

MTT assay for determining cytotoxicity of silver nanoparticles

The MTT assay was used to determine the cytotoxicity profile of silver nanoparticles as described with minor modification (Mosmann and Tim, 1983). Briefly, THP-1 cells (2×10^4 cells/ml) were seeded in 96-well plates and exposed to different concentrations (25µg/ml, 50µg/ml, 100µg/ml, 200µg/ml and 400µg/ml) of synthesised AgNPs and 250µg/ml of camphothecin for a period of 24 hours. After the treatment period, the cells were allowed to react with MTT for a period of 3–4 hours in dark at 37°C. At the end of the incubation period, dark purple formazan crystals were formed. These crystals were solubilized with an organic solvent before measuring the OD values at absorbance of 595 nm spectrophotometrically. Camphothecin was used as positive control for this experiment. To determine the cell viability, we calculated percent viability as % viability = [(Optical density {OD} of treated cell − OD of blank)/(OD of vehicle control − OD of blank) × 100]. Peripheral blood mononuclear cells (PBMC) were isolated from healthy human volunteer by Ficoll-Paque (Histopaque 1077, Himedia laboratories) using density gradient centrifugation as per standard procedure. PBMC (2×10^4 cells/well) were cultured in complete RPMI-1640 media as usual and incubated with different concentrations (25µg/ml, 50µg/ml, 100µg/ml, 200µg/ml and 400µg/ml) of synthesised AgNPs to evaluate cytotoxicity for 24 hours using MTT assay as described above. The Morphological changes were observed under phase contrast microscope.

DAPI staining and arcidine orange/Ethidium bromide dual staining to detect nucleic acid morphology

The morphology of nucleic acid material was monitored by fluorescent microscopy using DAPI staining method as described (Vivek et al., 2012). Briefly, the THP-1 cells (2×10^4 cells/ml) were added on a coverslip bottom dish and incubated for 24 h at 37°C in humidified atmosphere with 5% CO_2. After incubation, the cells were treated with five different concentrations (25µg/ml, 50µg/ml, 100 µg/ml, 200µg/ml and 400µg/ml) of AgNPs, exempting the control group, and were incubated for additional 24 h at the same conditions mentioned above. Then, the cells were washed

twice with 1x PBS, and DAPI solution (diluted in methanol) was added. The plates were wrapped with aluminium foil to protect from light and incubated for additional 15 min. The cells were fixed on the coverslip by using antifade reagent, and the nuclear material morphology was observed under a florescence microscope (Leica DM6B, Lecia microsystems). For AO/EB staining, Cells were seeded at a concentration of 2×10^5 cell/ml in 6-well tissue culture plates for arcidine organge/ ethidium bromine dual staining as described with minor modifications (Baharara et al., 2016). Following incubation, the medium was removed and replaced with phosphate-buffer saline (PBS) and supplemented with AgNPs with five different concentrations (25µg/ml, 50µg/ml, 100µg/ml, 200µg/ml and 400µg/ml) for both 24 h and 48 h. After the treatment period, cells were stained with AO/EB stain (1 mg/ml). After staining, the cells were visualized immediately under the fluorescence microscope (Leica DM6B, Lecia microsystems).

Annexin V FITC/PI dual staining apoptosis assay using flow cytometry

Apoptosis was assessed via flow cytometric analysis of control and AgNPs treated cells that were stained with FITC-Annexin V and PI using the Annexin V-FITC apoptosis detection kit according to the manufacturer's protocol (BD Bioscience)(Otsuki et al., 2010). Briefly, cells were treated with 150µg/ml and 400µg/ml of AgNPs for 24 hours at 37°C and 5% CO_2. Untreated cells were used as control. Subsequently, the cells were re-suspended in 500µl of 1X Annexin-binding buffer after washing with PBS. Then cells were incubated at room temperature with Annexin V-FITC and PI stain in the absence of light. Following the 10 minute incubation, samples were immediately analyzed via flow cytometry (FACSCalibur, BD Biosciences, San Jose, CA) using CellQuest 3.3 Software.

Cell cycle analysis using flow cytometry

Cell cycle perturbations were assessed using flow cytometry to measure the proportion of cells in different phases (Berkovich et al., 2013). Cell cycle perturbations induced by AgNPs were analyzed using propidium iodide DNA staining. Approximately 2×10^5suspension cells per well were plated in six-well plates and allowed to grow. After cells becomes 70% confluent, treated with 400 µg/ml AgNPs for 24 hours and then collected and fixed in ice-cold 70% ethanol for 4 hours and stored at 4°C until PI staining. Ethanol-suspended cells were then centrifuged at 1000 rpm for 5 min and washed twice in PBS to remove residual ethanol. Untreated cells are used as control. Pellets were suspended in 1 ml of PI/RNase A reagent and incubated at 37°C for 30 min. Cell cycle profiles were obtained using a BD FACScan Cell flow Cytometer (Becton Dickinson, USA). Debris and aggregates were gated out during data acquisition and data were analyzed with the Cell Quest Pro software.

Intracellular ROS measurement using fluorescent DCFDA dye

The generation of intracellular ROS was measured by florescence microscope using the oxidative sensitive fluorescent probe DCFDA as described with minor modifications (Mollik et al., 2014). DCFDA passively enters inside the cells and reacts with cellular ROS to form a highly florescent compound DCF (dichlorofluorescein). In brief, THP-1 cells were treated with five different concentrations (25µg/ml, 50µg/ml, 100µg/ml, 200µg/ml and 400µg/ml) of AgNPs and one untreated well (control) for 24 h. After the treatment, the cells were washed twice with sterile 1X PBS and incubated with culture medium containing 50µM of DCFDA for 1 h in the dark. Then, the cells were washed with sterile 1X PBS for three times to remove extracellular dye and harvested. The collected cells were resuspended in sterile 1X PBS. The image of cells were captured using florescent microscope (Leica DM6B, Lecia microsystems) with an excitation wavelength of 488 nm and an emission wavelength of 525 nm and the intensities were quantified using Image J software

Rhodamine 123/PI staining to measure mitochondrial membrane potential

The change in mitochondrial membrane potential was analyzed by using the fluorescent dyes such as rhodamine 123 (cationic green fluorescent dye) and PI (red-fluorescent dye) as described with minor modifications (Papaioannou, 1997). In brief, THP-1 cells were seeded in 6- well tissue culture plates and treated with five different concentrations (25µg/ml, 50µg/ml, 100µg/ml and 400µg/ml) of AgNPs and control as untreated well. After the treatment with AgNPs, the cells were washed twice with sterile 1X PBS and stained with rhodamine 123 (5µg/ml) and PI (5µg/ml) for 30 min at 37°C. After the incubation, the mitochondrial membrane potential was visualized by using fluorescence microscopy (Leica DM6B, Lecia microsystems) at excitation wavelength = 505 nm and emission wavelength = 534 nm for rhodamine 123 and excitation wavelength = 493 nm and emission wavelength = 617 nm for propidium iodide.

Caspase 3 colorimetric assay

Using the colorimetric protease assay ApoTarget Kit (BioSource International, Inc., CA) following the protocol of the manufacturer, the activity of caspase-3 was measured with minor modifications (Mantena et al., 2006). Briefly, the cells were treated with AgNP (400µg/ml) with or without pan-caspase inhibitor (z-VAD-fmk). The z-VAD-fmk (60µmol/L) was added 2 hours before the addition of the AgNP. The cells were harvested using trypsinization and cell lysates prepared as described. Samples of the cell

lysates (100 Ag protein per sample) were mixed with reaction buffer and 200 Amol/L substrate (DEVD-pNA for caspase-3) and incubated for 3 hours at 37°C in the dark. The absorbance was then measured at 405 nm and the sample readings calculated by subtracting the absorbance of blank samples.

DNA fragmentation assay

In order to confirm the caspase 3 upregulation, DNA fragmentation was done as described with modifications (Islam et al., 2015). The THP-1 cells with density of 1×10^6/ml were plated per well of six-well tissue culture plates and incubated at 37°C/5% CO_2 overnight. These cells were treated with 2.0 mL of stock solution. Cells were treated with five different concentrations (25µg/ml, 50µg/ml, 100µg/ml, 200µg/ml and 400µg/ml) of AgNps and one untreated control. The cell pellets were treated for 10 s with 50µL of lysis buffer (1% NP-40 in 20 mM EDTA, 50 mM Tris-HCl, pH 7.5). After centrifugation for 5 min at 1600× g (unit rotations per minute) the supernatant was collected and the extraction was repeated with the same amount of lysis buffer. With the supernatant, an additional amount of Sodium dodecyl sulphate (SDS) was added to final concentration of 1% and treated for 2 h with RNase A (final concentration 5µg/µL) at 56°C followed by digestion with proteinase K (final concentration 2.5µg/µL) for 2 h at 37°C. By the addition of 1/2µL 10 M ammonium acetate, DNA resulted in precipitated form with 2.5µL ethanol for obtaining the DNA in a purified form. The DNA pellet was fused in 50µL of TE buffer, and separated by electrophoresis in 1.0% agarose gel. DNA electrophoresis was performed in 1% agarose gel containing 1µg /mL ethidium bromide at 70 V, and the DNA segments were visualized by exposing the gel to ultraviolet light, along with photography.

Statistical analysis

All experimental results were expressed as the mean ± standard deviation (SD). Statistical significance was calculated by One Way ANOVA using GraphPad 7.0 software by Prism Inc. P value of less than 0.05 was considered to be statistically significant.

Results

Phytochemical analysis of leaf extract

The phytochemical analysis using biochemical tests showed the presence of carbohydrats, flavonoids, saponins, tannins, glycosides, terpenoids, alkaloids, phenol and protiens. Resins and steroids showed negative result.

Characterization of silver nanoparticles

The absorption spectra of the AgNPs is shown in figure 1-A. The sample showed the characteristic Surface-Plasmon peak at 420 nm. The appearance of peak at 400nm - 430nm reveals the formation of silver nanoparticles. The XRD patterns of AgNPs resulted in the diffraction peaks at 2θ degree of 38.08, 44.13,

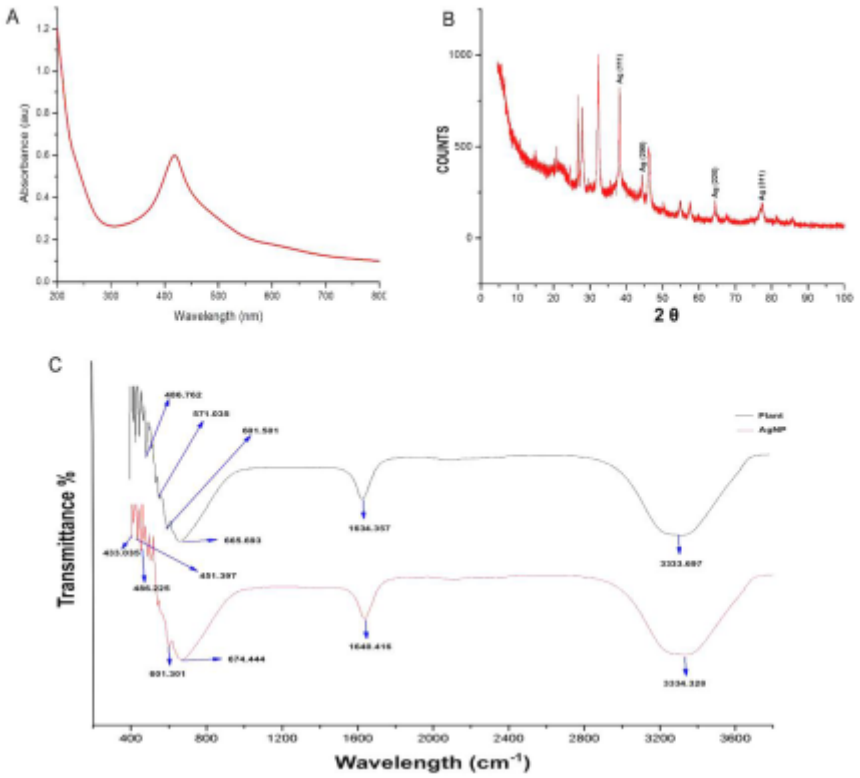

Figure 1: A) UV-vis spectroscopy of silver nanoparticles shows peak at 400 nm – 420 nm range, B) XRD pattern of silver nanoparticles shows FCC structure of silver nanoparticles and C) FTIR peaks of silver nanoparticle and leaf extract.

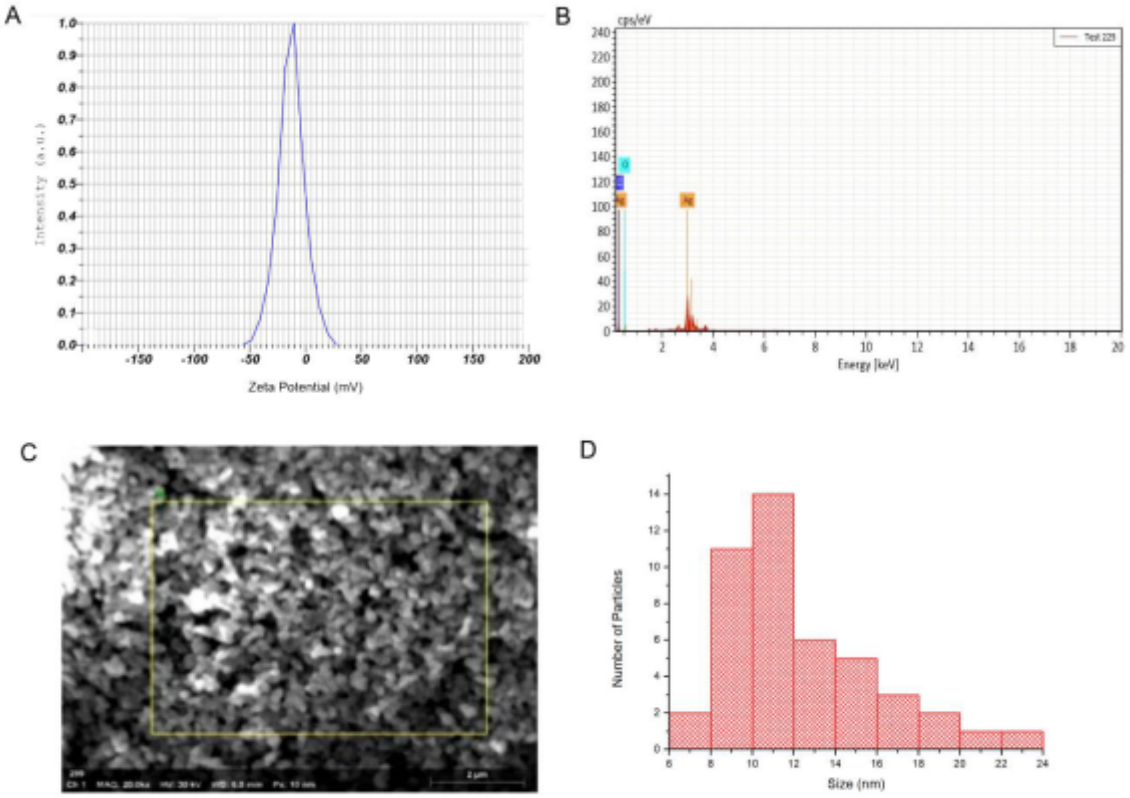

Figure 2. A) Zeta potential of silver nanoparticle B) EDX chromatogram of silver nanoparticle, C) FESEM image of silver nanoparticle, D) Size analysis of silver nanoparticle.

64.63 and 77.14 which corresponds to the hkl planes of (111), (200), (220), and (311) respectively (Figur 1-B). All of the main peaks were indexed as AgNPs with the face centered cubic (fcc) lattice of silver, by comparing with the standard data (JCPDS file No.01-071-4613). FTIR spectrum of AgNPs and leaf extract (Figure 1-C)shows peaks at 3334.328 cm^{-1}, 1640 cm^{-1}, 673.444 cm^{-1}, 601.301 cm^{-1}, 486.225 cm^{-1}, 451.397 cm^{-1}, 433.035 cm^{-1} which corresponds to O-H stretch, C-C stretch, N-H wag, PO4 3-, COO- rocking, symmetric bending of O-Al-O and C-Br stretch respectively. There is upshift in wavelength 3334.328 cm^{-1} in nanoparticle from wavelength in leaf extract at 3333.697 cm^{-1} which shows compounds in leaves have lost their molecules to aid in formation of nanoparticles. There is another instance where another upshift in wavelength can be seen at 1640.416 cm^{-1} in nanoparticle from 1634.357 cm^{-1} in leaf extract. These FTIR spectroscopic studies confirmed that there are many interactions between leaf extract and silver nitrate leading to formation of silver nanoparticles and also strong binding ability with metal suggested the formation of layer covering metal nanoparticles. Thus plant extract acts as stabilizing and reducing agent in formation of silver nanoparticles. The zeta potential analysis revealed the nanoparticle charge as -12.9 Mv (Figure 2-A) which shows that nanoparticles possess negative charge on its surface and Energy dispersive X-Ray (EDX) analysis shows that Ag is the highest composition element along with carbon and oxygen elements (Figure 2-B).The size, shape and morphology of the green synthesized AgNPs were further characterized by FESEM analysis that showed individual AgNPs have predominantly spherical geometry (Figure 2-C) with particles in size range of 6 nm to 24 nm (Figure 2-D).

Silver nanoparticles decrease cell viability of THP-1 cells in concentration dependent manner

The MTT assay shows that synthesized silver nanoparticles can effectively inhibit the survival of THP-1 cells in vitro. The MTT assay revealed concentration dependent cell viability decrease in THP-1 cell lines (Figure 3-B). The five different concentrations (25µg/ml, 50µg/ml, 100µg/ml, 200µg/ml and 400µg/ml) of silver nanoparticles tested on THP-1 cell lines showed cell viability of 91±2 % (no significance), 74±0.8% ($p=0.48$), 55±1.2% ($p<0.001$), 29±1.9% ($p<0.001$) and 10±0.04% ($p<0.001$) respectively. The positive control campothecin at 250µg/ml showed 51±0.7% cell viability. The silver nanoparticle concentrations at 200µg/ml and 400µg/ml showed great decrease in cell viability than campothecin which proves that silver nanoparticles has great cytotoxic effect towards THP-1 cells than positive control. Further synthesized silver nanoparticles showed very less cytotoxicity towards

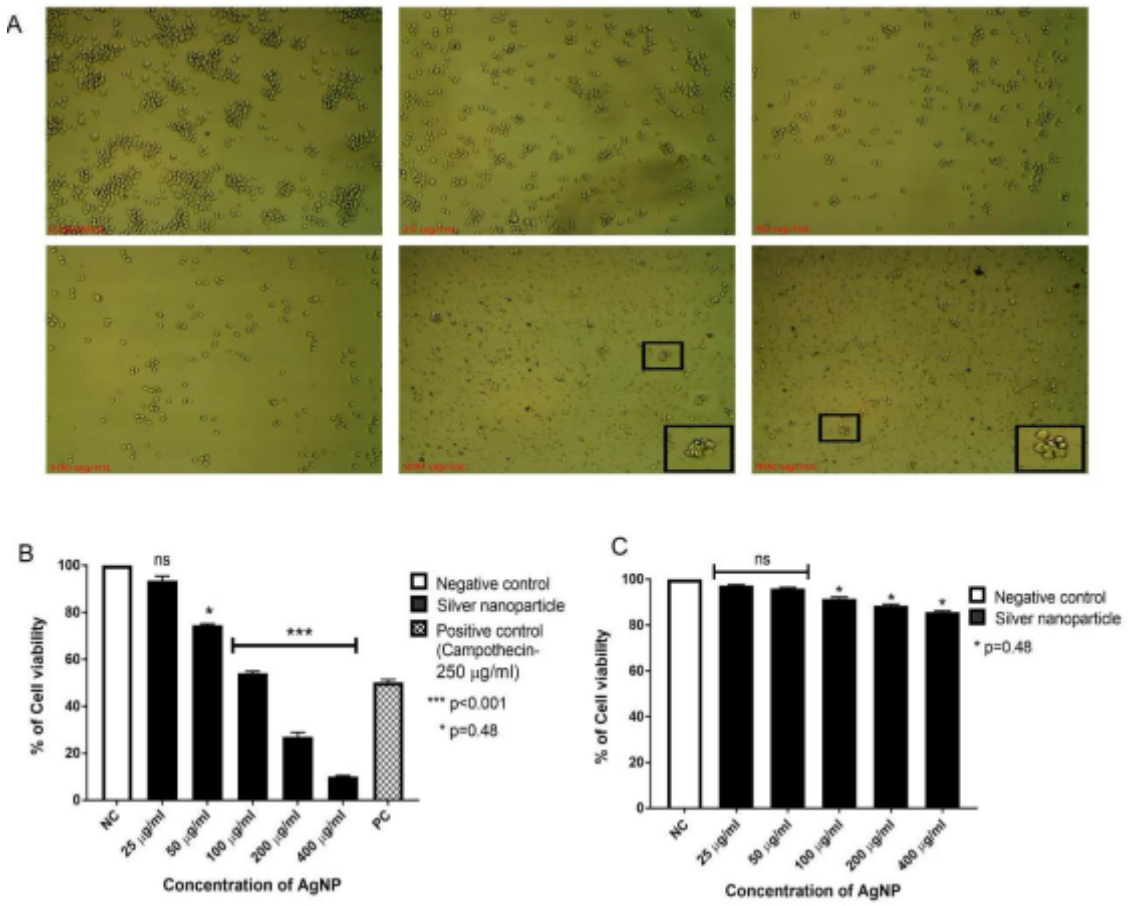

Figure 3. A) THP-1 cells visualized under phase contrast microscope with and without silver nanoparticles treatment, B) MTT assay graph of silver nanoparticle effect on THP-1 cell lines, C) MTT assay graph of silver nanoparticle effect on peripheral blood mononuclear cells.

normal peripheral blood mononuclear cells (Figure 3- C). The five different concentrations (25µg/ml, 50µg/ml, 100µg/ml, 200µg/ml and 400µg/ml) of silver nanoparticles showed cell viability in PBMC cells of 96±1.3 % (no significance), 94±1.1% (no significance), 90±0.9% (p=0.48), 87±1% (p=0.48) and 84±0.68% (p=0.48) respectively. However, cell viability didn't fall below 50% which shows that silver nanoparticles are very less toxic to normal cells but are high cytotoxic to THP-1 cells. The morphological observation under phase contrast microscope also reveals change in cell shape and cell clumping along with decrease number of cells with increase in concentration of AgNPs (Figure 3-A).

DAPI staining and AO/EB dual staining revealed apoptotic morphology

Florescence microscopic images (Figure 4) showed the DAPI staining of THP-1 cells. Synthesized silver nanoparticles induced morphological changes such as cell shrinkage, rounding of cells and membrane blebbing which depict the induction of apoptosis (represented in red arrow). It was noted that there were more apoptotic cells (showing fragmented nucleus)in nanoparticles treated groups than the control (untreated cells). It is clearly evident that different concentration of silver nanoparticles (25µg/ml, 50µg/ml, 100µg/ml, 200µg/ml and 400µg/ml) has induced nuclear morphological changes and DNA condensation in cells with varying intensity in concentration dependent manner. AO/EB dual staining was performed on THP-1 cells treated with all five concentrations of synthesized silver nanoparticles for 24 hours (Figure 5- A) and 48 hours (Figure 5- B). Based on apoptotic cell feature, number of apoptotic cells was counted (Figure 6). At 24 hours, the number of apoptotic cells in five different concentrations are as 22±2.8%, 46±2.3%, 65±1.8%, 78±1.13% and 94±0.57% respectively. At 48 hours, increase in apoptotic cells can be observed, 36±1.2%, 57±1.5%, 72±0.8%, 82±0.24% and 95.3±0.13%, respectively. Control cells showed no apoptotic cells.

Silver nanoparticles administration to THP-1 cells increase apoptotic cell population

To further confirm the role of silver nanoparticles on inducing apoptosis, THP-1 cells were treated with two different concentrations nanoparticles (150µg/ml and 400µg/ml) of AgNPs for 24 hours followed by staining with Annexin V-FITC and PI to determine the percentage of cells undergo apoptosis. The untreated cells that didn't receive

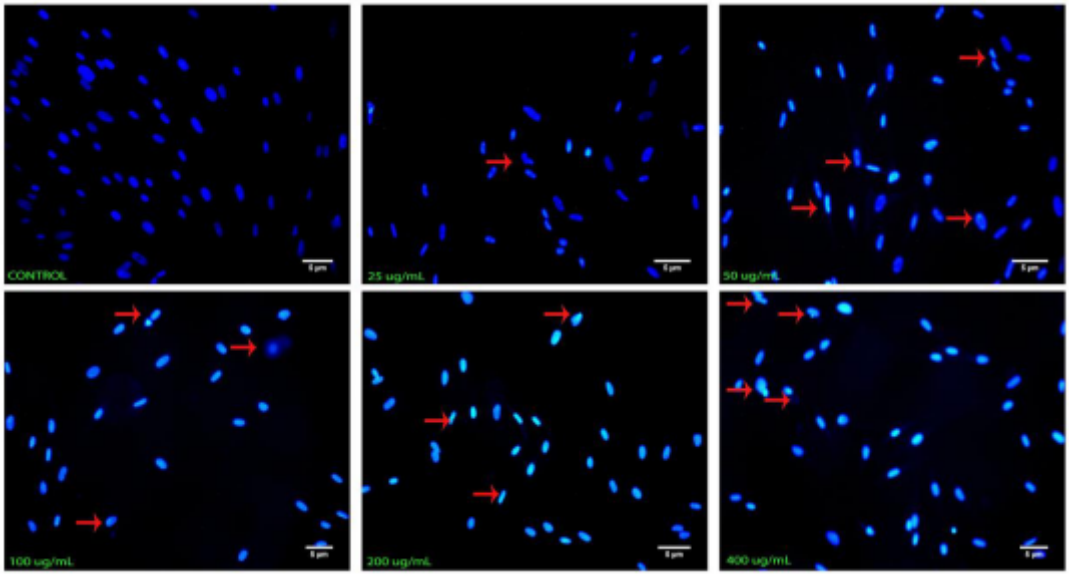

Figure 4. DAPI staining of THP-1 cells with and without administration of silver nanoparticles. (Red arrow shows apoptotic cells caused by silver nanoparticles).

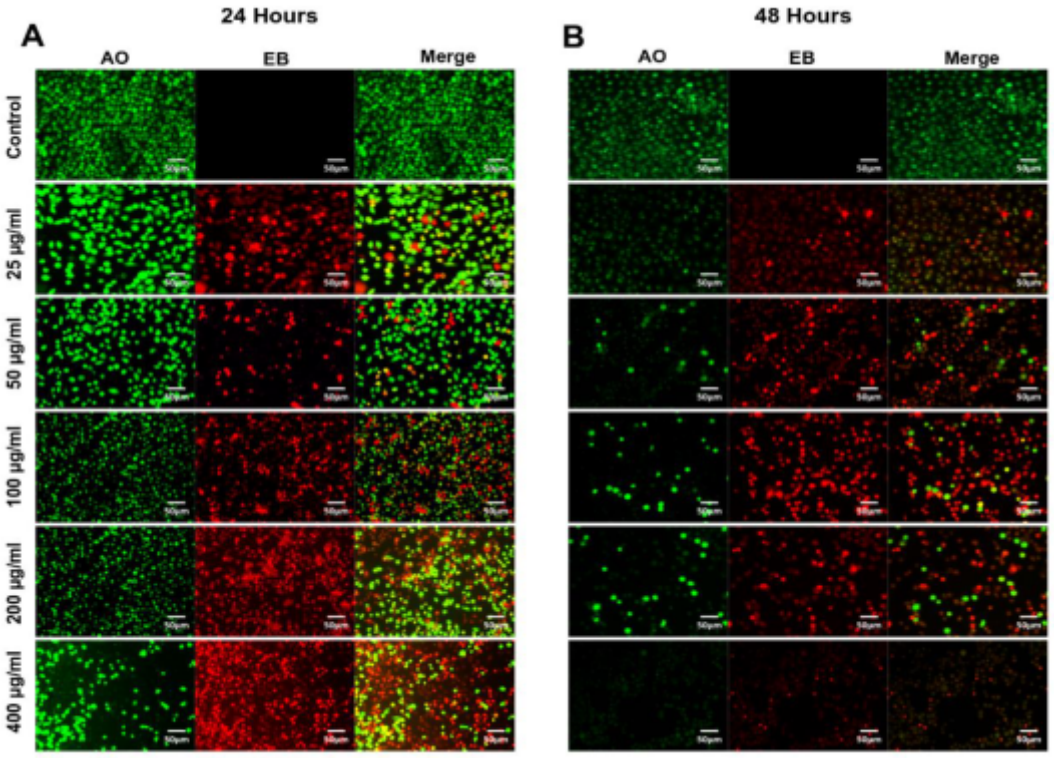

Figure 5. A) Arcidine orange/Ethidium bromide staining of THP-1 cells with and without silver nanoparticles administration after 24 hours, B) Arcidine orange/Ethidium bromide staining of THP-1 cells with and without silver nanoparticles administration after 48 hours.

treatment to AgNPs were control. The flow cytometry results are shown in figure 7- A. From figure 7- B, It can be seen that the percentage of live cells are more in control than in treated groups. The control cells, 150µg/ml treated cells and 400µg/ml treated cells show 99±0.3 %, 43±1.3% and 8±0.2% live cells (Annexin V positive, PI negative) respectively. The percentage of early apoptotic cells present in control cells, 150µg/ml treated cells and 400µg/ml treated cells are 0.06±0.02%, 47.35±0.76% and 1±0.24% respectively (Figure 7- C). The percentage of late apoptotic cells (Annexin V positive, PI positive) in 150µg/ml treated cells and 400µg/ml treated cells are 7.76±0.4% and 83.65±0.87% respectively (Figure 7- D). The control cells showed no late apoptotic cells as they were not treated with silver nanoparticles. There are also very few

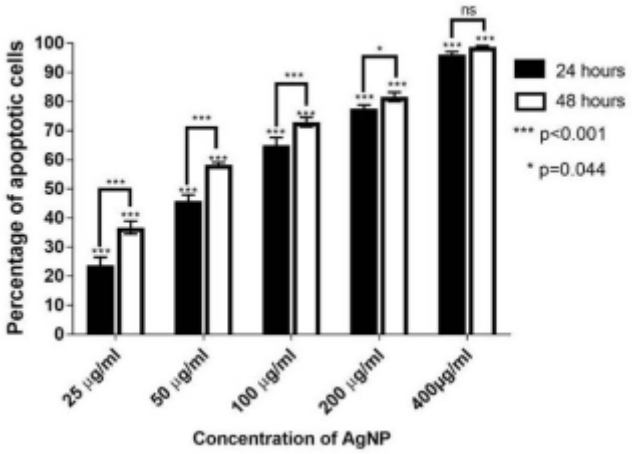

Figure 6. Apoptotic cells count graph of THP-1 cells that were dual stained with arcidine orange/ethidium bromide.

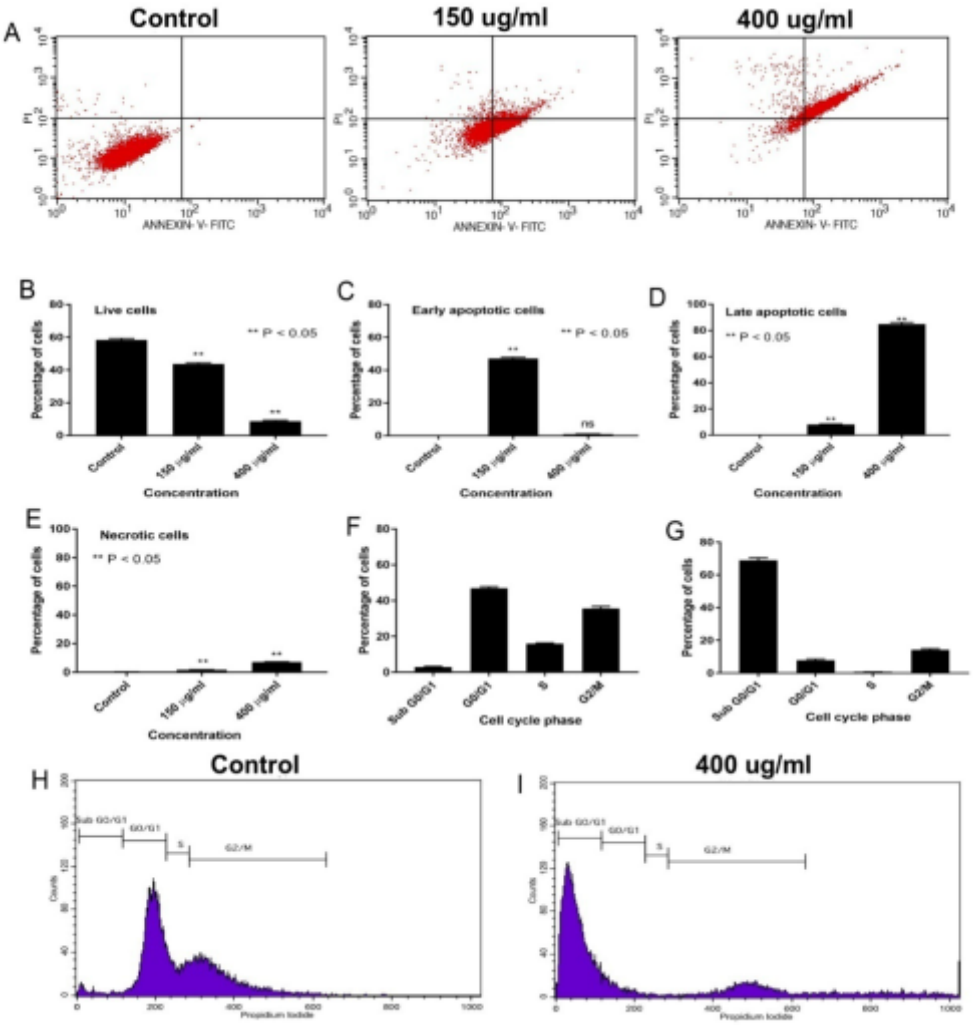

Figure 7. A) Dot plot of Annexin V FITC/ PI staining using flow cytometry of THP-1 cells with and without silver nanoparticle adminsitration, B) Graph showing quantification of live cells in Annexin V- FITC/PI experiment, C) Graph showing quantification of early apoptotic cells in Annexin V- FITC/PI experiment, D) Graph showing quantification of late apoptotic cells in Annexin V- FITC/PI experiment, E) Graph showing quantification of necrotic cells in Annexin V- FITC/PI experiment, F) Graph showing quantification of cell population in different cell cycle phase in control cells, G) Graph showing quantification of cell population in different cell cycle phase in400 µg/ml AgNPs treated THP-1 cells, H) Cell cycle histogram of control cells showing less population in Sub G0/G1 phase, I) Cell cycle histogram of 400 µg/ml AgNPs treated THP-1 cells showing cell cycle arrest at sub G0/G1 cell cycle phase indicating apoptosis. Statistical analysis represented in this figure *p=0.48, **p<0.05, ***p<0.001.

necrotic cells population which makes up to 0.30±0.12%, 1.63±0.92%, 6.98±0.35% in control cells, 150µg/ml treated cells and 400µg/ml treated cells respectively (Figure 7- E). This confirms that silver nanoparticles induce apoptosis in THP-1 cells in concentration dependent manner.

Silver nanoparticles arrest cell cycle at Sub G0/G1 phase

Following apoptosis study, flow cytometry with PI staining was performed to investigate the cell cycle arrest in THP-1 cells treated with synthesized silver nanoparticles. The cell cycle analysis chromatogram for control and 400µg/ml AgNPs treated cells are shown in figure 7- H & figure 7- I respectively. It can be seen in control cells (Figure 7- F) that there are cell population of 2.5±0.32% in Sub G0/G1 phase, 47.55±0.2% in G0/G1 phase, 15.61±0.7 % in S phase and 34.85±1.2% in G2/M phase. The less number of cells in Sub G0/G1 phase and more population of cells in other phases indicates that cells are actively dividing when not treated with silver nanoparticles. In contrast, the treated cells show cell population of 67.88±1.3 % in Sub G0/G1 phase, 7.47±0.43 % in G0/G1 phase, 0.65±0.1% in S phase and 14.69±0.6% in G2/M phase (Figure 7- G). This shows that there is increase in cell population at Sub G0/G1 phase with decrease in cell population in other phases. This indicates that cell cycle arrest at Sub G0/G1 phase and it's a confirmed feature of apoptosis.

Intracellular ROS increased in concentration dependent manner upon administration of silver nanoparticles

Since the generation of ROS is associated with apoptosis, the intercellular ROS levels in AgNPs-treated THP-1 cells were investigated through oxidation-sensitive DCF fluorescence intensity observed under florescence microscope (Figure 8- A) and quantified (Figure 8- B). The non-fluorescent DCFDA easily permeabilized through cell membrane and got oxidized into highly fluorescence DCF in the presence of ROS. The increase in fluorescence intensity shows the increase in intracellular ROS formation in the cell. The silver nanoparticles concentration-dependent significant increase (p=0.0001) in DCF fluorescence was detected in treated cells. This proves that silver nanoparticle induce ROS formation as important mechanism towards inducing apoptosis.

Silver nanoparticles alters mitochondrial membrane permeability

ROS mediated apoptotic signaling leads to alteration of mitochondrial membrane potential in cells. THP-1 cells were treated with five different concentration of silver nanoparticles for 24. Then cells were dual stained with rhodamine 123 and PI to detect changes in the mitochondrial membrane potential. As shown in Figure 9- A, we observed significant changes in the activity of the mitochondrial membrane potential in THP-1 cells after AgNP treatment in a concentration dependent manner. There is decrease in florescence intensity in as concentration of AgNP treatment to cells increases which shows mitochondrial depolarization occurs (Figure 9-B). The PI staining increases with increase in concentration of AgNPs treatment as cells undergo death

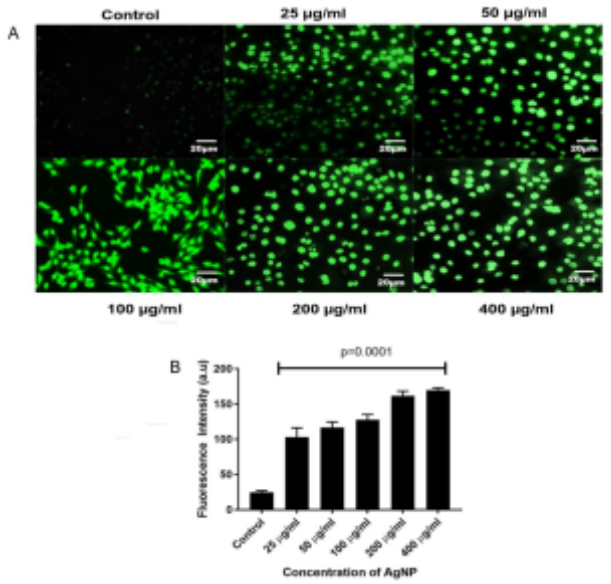

Figure 8. A) DCFDA staining images of THP-1 cells to measure intracellular reactive oxygen species, B) Florescence intensity graph of DCFDA staining of control cells and treated cells.

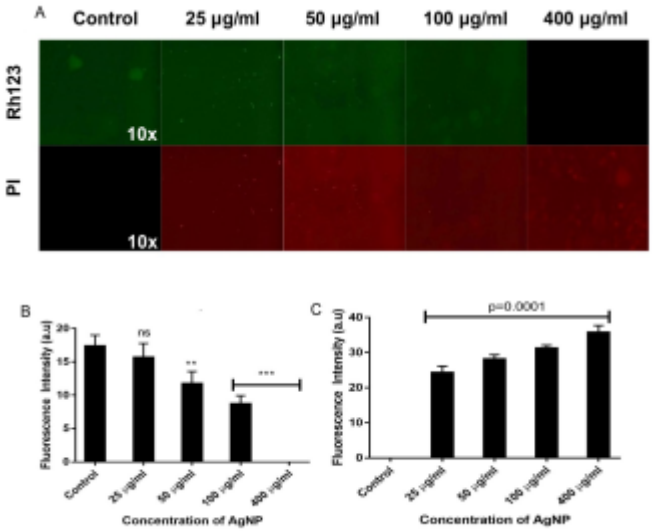

Figure 9: A) Fluorescent microscope images of Rhodamine 123 staining and Propidium iodide staining of THP-1 cells, B) Fluorescent intensity graph of Rhodamine 123 staining, C) Fluorescent intensity graph of propidium iodide staining. **p<0.05, ***p<0.001

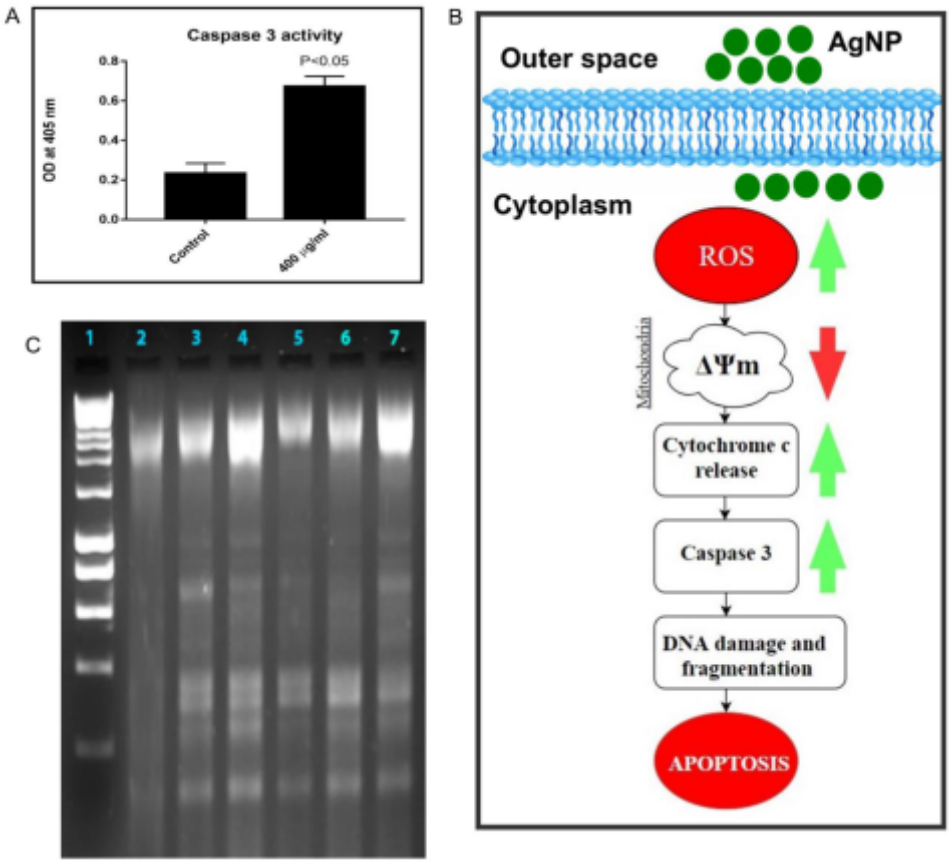

Figure 10. A) Graph showing colorimetric caspase 3 activity, B) Possible mechanism of action of silver nanoparticles, C) DNA fragmentation assay reveals that DNA is fragmented upon silver nanoparticle administration.

which could be due to depolarization of mitochondria (Figure 9-C). These results suggest that ROS released upon AgNPs administration alters the mitochondrial membrane potential thereby inducing apoptosis in THP-1 cells.

Silver nanoparticles upregulate caspase 3 level in THP-1 cells

The caspase 3 activation is determined calorimetrically (Figure 10-A). The cells treated with silver nanoparticles and pan-caspase inhibitor (z-VAD-fmk), silver nanoparticles without pan-caspase inhibitor (z-VAD-fmk) and untreated cells as control are three assay conditions investigated. In the presence of pan-caspase inhibitor (z-VAD-fmk), there is decrease in optical density (data not shown) but in the absence of pan-caspase inhibitor (z-VAD-fmk), there is significant increase ($p<0.05$) in caspase activity resulting in high OD value compared to the control. This shows that synthesized silver nanoparticles activate the caspase 3 pathway to induce apoptosis. From the entire experiments we can conclude that nanoparticles increase the intracellular reactive oxygen species. These results in mitochondrial depolarization releasing cytochrome c that is required to upregulate caspase 3 (Figure 10- B).

DNA fragmentation is induced by silver nanoparticles

DNA fragmentation is one of thecharacteristic of caspase mediated apoptosis. As shown in figure 10- C, Lane 1 shows 1.5 Bp ladder, lane 2 shows negative control, lane 3 to lane 7 shows silver nanoparticles treated cell laddering at all five different concentrations (25µg/ml, 50µg/ml, 100µg/ml, 200µg/ml and 400µg/ml) respectively. It can be noted that all five different concentrations of silver nanoparticle markedly induced DNA fragmentation in THP-1 cells. However, untreated cells didn't show any fragmentation which proves that silver nanoparticles are required to induce fragmentation of DNA thereby leading to apoptosis. This could be due to the extremely increased generation of ROS by varying concentration of silver nanoparticles treatment in THP-1 cells.

Conclusion

Thus, the current study investigated the mechanism of action of *A. Barbadensis* mediated synthesis of silver nanoparticles and their anti-leukemic property *in vitro*. The synthesized silver nanoparticles induced showed significant anti-leukemic potential than that of standard drug by inhibiting the proliferation of THP-1 cells through apoptotic mechanism. Taken together, our results suggest that synthesized silver nanoparticle would become a standard

anti-leukemic therapy in the future due to many advantages over current treatment as synthesizing the leaf mediated synthesis of silver nanoparticles are very cheap, takes less time to synthesize, no need of complex equipment, can be applied for large scale production. Further studies like gene expression analysis and *in vivo* studies should be established in future.

Acknowledgments

The authors express gratefulness to the SRM Institute of Science and Technology (Formerly known as SRM University) for providing equipment and other facilities to execute this study. The authors thank the Nanotechnology Research Centre, SRM University for nanoparticle characterization facilities. The authors thank Dr. M.R. Ganesh, IIISM, SRMIST for providing the THP-1 cell lines for the *in vitro* study.

Disclosure

The author reports no conflicts of interest in this work.

References

Al-Mefty O, Kersh JE, Routh A, Smith RR. 1990. The long-term side effects of radiation therapy for benign brain tumors in adults. Journal of Neurosurgery 73(4):502-12512.

AshaRani PV, Low Kah Mun G, Hande MP, Valiyaveettil S. 2008. Cytotoxicity and genotoxicity of silver nanoparticles in human cells. ACS nano 3: 279.

Azizi S, Ahmad MB, Namvar F, Mohamad R. 2014. Green biosynthesis and characterization of zinc oxide nanoparticles using brown marine macroalga Sargassum muticum aqueous extract. Materials Letters 116: 275–277.

Baharara J, Ramezani T, Divsalar A, Mousavi M, Seyedarabi A. 2016. Induction of Apoptosis by Green Synthesized Gold Nanoparticles Through Activation of Caspase-3 and 9 in Human Cervical Cancer Cells. Avicenna Journal of Medical Biotechnology 8:75.

Berkovich L, Earon G, Ron I, Rimmon A, Vexler A, Lev-Ari S. 2013. Moringa Oleifera aqueous leaf extract down-regulates nuclear factor-kappaB and increases cytotoxic effect of chemotherapy in pancreatic cancer cells. BMC complementary and alternative medicine 13:212.

Bhandary SK, Kumari S, Bhat VS, Sharmila KP, Bekal MP. 2012. Preliminary phytochemical screening of various extracts of Punica granatum peel, whole fruit and seeds. Journal of Health Sciences 2:34-35.

Biener J, Wittstock A, Baumann T, Weissmüller J, Bäumer M, Hamza A. 2009. Surface chemistry in nanoscale materials. Materials 2(4): 2404-2428.

Curtis RE, Boice JD, Moloney WC, Ries LG, Flannery JT. Leukemia following chemotherapy for breast cancer (1990). Cancer Research 50(9):2741-6.

Deininger Michael WN, Druker BJ. 2003. Specific targeted therapy of chronic myelogenous leukemia with imatinib. Pharmacological Reviews 55(3):401-23.

Duffner Patricia K. 2004. Long-term effects of radiation therapy on cognitive and endocrine function in children with leukemia and brain tumors. The neurologist 10(6):293-310.

Elumalai EK, Prasad TNVKV, Venkata K, Nagajyothi PC, David E. 2010. Green synthesis of silver nanoparticle using Euphorbia hirta L and their antifungal activities. Archives of Applied Science Research 2 (6): 76-81.

Foon KA, Zighelboim J, Yale C, Gale RP. 1981. Intensive chemotherapy is the treatment of choice for elderly patients with acute myelogenous leukemia. Blood 58(3):467-70.

Galdiero S, Falanga A, Vitiello M, Cantisani M, Marra V, Galdiero M. 2011. Silver nanoparticles as potential antiviral agents. Molecules 16(10):8894-918.

Ghule K, Ghule AV, Chen BJ, Ling YC. 2006. Preparation and characterization of ZnO nanoparticles coated paper and its antibacterial activity study. Green Chemistry 8:1034-1041.

Haiss W, Thanh NT, Aveyard J, Fernig DG. 2007. Determination of size and concentration of gold nanoparticles from UV− Vis spectra. Analytical chemistry 79(11):4215-4221.

Holleman A, Cheok MH, den Boer ML, Yang W, Veerman AJ, Kazemier KM, Pei D, Cheng C, Pui CH, Relling MV, Janka-Schaub GE. 2004. Gene-expression patterns in drug-resistant acute lymphoblastic leukemia cells and response to treatment. New England Journal of Medicine 351:533-542.

Horowitz MM, Gale RP, Sondel PM, Goldman JM, Kersey J, Kolb HJ, Rimm AA, Ringden O, Rozman C, Speck B. 1990. Graft-versus-leukemia reactions after bone marrow transplantation. Blood 75(3):555-62.

Islam F, Raihan O, Chowdhury D, Khatun M, Zuberi N, Khatun L, Brishti A, Bahar E. 2015. Apoptotic and antioxidant activities of methanol extract of Mussaenda roxburghii leaves. Pakistan journal of pharmaceutical sciences 28(6):2027-34.

Jain P, Pradeep T. 2005. Potential of silver nanoparticle-coated polyurethane foam as an antibacterial water filter. Biotechnology and bioengineering 90(1):59-63.

Jiang J, Oberdörster G, Biswas P. 2009. Characterization of size, surface charge, and agglomeration state of nanoparticle dispersions for toxicological studies. Journal of Nanoparticle Research 11:77.

Jo Young-Ki, Kim BH, Jung G. 2009. Antifungal activity of

silver ions and nanoparticles on phytopathogenic fungi. Plant Disease 93(10): 1037-1040.

Kaldor JM, Day NE, Pettersson F, Clarke EA, Pedersen D, Mehnert W, Bell J, Høst H, Prior P, Karjalainen S, Neal F. 1990. Leukemia following chemotherapy for ovarian cancer. New England Journal of Medicine 322:1-6.

Khan I, Saeed K, Khan I. 2017. Nanoparticles: Properties, applications and toxicities. Arabian Journal of Chemistry 15:101.

Krishnaraj C, Jagan EG, Rajasekar S, Selvakumar P, Kalaichelvan PT, Mohan N. 2010. Synthesis of silver nanoparticles using Acalypha indica leaf extracts and its antibacterial activity against water borne pathogens. Colloids and Surfaces B: Biointerfaces 76(1):50-6.

Lara HH, Ayala-Nuñez NV, Ixtepan-Turrent L, Rodriguez-Padilla C. 2010. Mode of antiviral action of silver nanoparticles against HIV-1. Journal of Nanobiotechnology 8:1.

Lewis Edward B. 1957. Leukemia and ionizing radiation. Science 125(3255):965-72.

Lin J, Zhou W, Kumbhar A, Wiemann J, Fang J, Carpenter EE, O'connor CJ. 2001. Gold-coated iron (Fe@ Au) nanoparticles: synthesis, characterization, and magnetic field-induced self-assembly. Journal of Solid State Chemistry 159(1):26-31.

Lu Y, Yin Y, Mayers BT, Xia Y. 2002. Modifying the surface properties of superparamagnetic iron oxide nanoparticles through a sol− gel approach. Nano letters 2(3): 183-186.

Lung JK, Huang JC, Tien DC, Liao CY, Tseng KH, Tsung TT, Kao WS, Tsai TH, Jwo CS, Lin HM, Stobinski L. 2007. Preparation of gold nanoparticles by arc discharge in water. Journal of Alloys and Compounds 472(1-2), 446–450.

Mantena SK, Sharma SD, Katiyar SK. 2006. Berberine, a natural product, induces G1-phase cell cycle arrest and caspase-3-dependent apoptosis in human prostate carcinoma cells. Molecular Cancer Therapeutics 5(2):296-308.

Mollick MMR, Bhowmick B, Mondal D, Maity D, Rana D, Dash SK, Chattopadhyay S, Roy S, Sarkar J, Acharya K, Chakraborty M. 2014. Anticancer (in vitro) and antimicrobial effect of gold nanoparticles synthesized using Abelmoschus esculentus (L.) pulp extract via a green route. RSC Advances 4: 37838-37848.

Mosmann Tim. 1983. Rapid colorimetric assay for cellular growth and survival: application to proliferation and cytotoxicity assays. Journal of Immunological Methods 65(1-2):55-63.

Narayanan KB, Natarajan S. 2010. Biological synthesis of metal nanoparticles by microbes. Advances in Colloid and Interface Science 156(1-2):1-13.

Otsuki N, Dang NH, Kumagai E, Kondo A, Iwata S, Morimoto C. 2010. Aqueous extract of Carica papaya leaves exhibits anti-tumor activity and immunomodulatory effects. Journal of Ethnopharmacology 127(3):760-7.

Papaioannou KZ. 1997. Assessment of viability and mitochondrial function of equine spermatozoa using double staining and flow cytometry. Theriogenology 48(2):299-312.

Rai Mahendra, Yadav A, Gade A. 2009. Silver nanoparticles as a new generation of antimicrobials. Biotechnology advances 27(1):76-83.

Sahu PK, Giri DD, Singh R, Pandey P, Gupta S, Shrivastava AK, Kumar A, Pandey KD. 2013. Therapeutic and medicinal uses of Aloe vera: a review. Pharmacology & Pharmacy 4: 599-610.

Sharma VK, Yngard RA, Lin Y. 2009. Silver nanoparticles: green synthesis and their antimicrobial activities. Advances in Colloid and Interface Science 145: 83-96.

Singh M, Singh S, Prasad S, Gambhir IS. 2008. Nanotechnology in medicine and antibacterial effect of silver nanoparticles. Digest Journal of Nanomaterials and Biostructures 3(3):115 - 122.

Snyder R. 2012. Leukemia and benzene. International journal of environmental research and public health 9(8):2875-93.

Subhashini S, Narayanan S, Rejani K, Kamath AT, Kamak DH, Aravind A. 2017. Studies on the in vitro antihepatotoxic activity of Indigofera tinctoria (Linn.) against Hep G2 Human liver carcinoma cell lines. Journal of Pharmacy Research 11:1086-94.

Tian J, Wong KK, Ho CM, Lok CN, Yu WY, Che CM, Chiu JF, Tam PK. 2007. Topical delivery of silver nanoparticles promotes wound healing. ChemMedChem 2(1):129-36.

Vivek R, Thangam R, Muthuchelian K, Gunasekaran P, Kaveri K, Kannan S. 2012. Green biosynthesis of silver nanoparticles from Annona squamosa leaf extract and its in vitro cytotoxic effect on MCF-7 cells. Process Biochemistry 47: 2405-2410.

What you need to know about leukemia. National Cancer Institute. Accessed Aug. 9, 2017 Available from URL: http://www.cancer.gov/publications/patient-education/wyntk-leukemia.

Yan XJ, Xu J, Gu ZH, Pan CM, Lu G, Shen Y, Shi JY, Zhu YM, Tang L, Zhang XW, Liang WX. 2011. Exome sequencing identifies somatic mutations of DNA methyltransferase gene DNMT3A in acute monocytic leukemia. Nature genetics 43(4):309-15.